ACSNANO
www.acsnano.org
ARTICLE

Enhanced Solar Cell Conversion Efficiency of InGaN/GaN Multiple Quantum Wells by Piezo-Phototronic Effect

Chunyan Jiang,[†,‡,§,⊥] Liang Jing,[†,‡,§,⊥] Xin Huang,[†,‡,§] Mengmeng Liu,[†,‡,§] Chunhua Du,[†,‡] Ting Liu,[†,‡,§] Xiong Pu,[†,‡] Weiguo Hu,[*,†,‡] and Zhong Lin Wang[*,†,‡,∥]

[†]Beijing Institute of Nanoenergy and Nanosystems, Chinese Academy of Sciences, Beijing 100083, China
[‡]CAS Center for Excellence in Nanoscience, National Center for Nanoscience and Technology (NCNST), Beijing 100190, China
[§]University of Chinese Academy of Sciences, Beijing 100049, China
[∥]School of Material Science and Engineering, Georgia Institute of Technology, Atlanta, Georgia 30332, United States

Supporting Information

ABSTRACT: **The piezo-phototronic effect is the tuning of piezoelectric polarization charges at the interface to largely enhance the efficiency of optoelectronic processes related to carrier separation or recombination. Here, we demonstrated the enhanced short-circuit current density and the conversion efficiency of InGaN/GaN multiple quantum well solar cells with an external stress applied on the device. The external-stress-induced piezoelectric charges generated at the interfaces of InGaN and GaN compensate the piezoelectric charges induced by lattice mismatch stress in the InGaN wells. The energy band realignment is calculated with a self-consistent numerical model to clarify the enhancement mechanism of optical-generated carriers. This research not only theoretically and experimentally proves the piezo-phototronic effect modulated the quantum photovoltaic device but also provides a great promise to maximize the use of solar energy in the current energy revolution.**

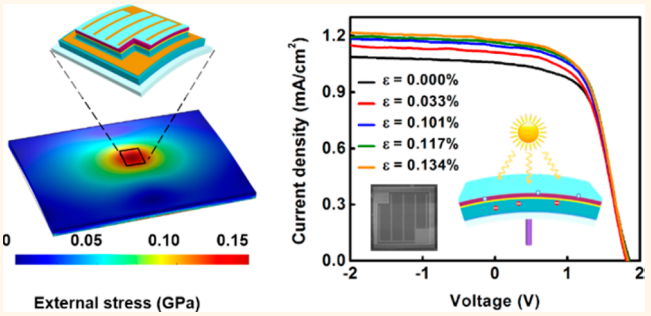

KEYWORDS: *solar cell, piezo-phototronic effect, InGaN/GaN multiple quantum wells, optical absorption, conversion efficiency*

The III-Nitride semiconductors such as InN, AlN, GaAs, and GaN have been intensively investigated for optoelectronics applications owing to their favorable physical properties.[1,2] Compared with Si, Ge, and the GaAs system, $In_xGa_{1-x}N$ is very attractive for designing multiple quantum well (MQW) solar cells due to the widest adjustment of direct and tunable band gap ranging from 0.7 eV for InN up to 3.4 eV for GaN. Moreover, the literature indicate that InGaN alloys have a high absorption coefficient ($>10^5$ cm^{-1} at the band edge),[3−5] which is suitable for both terrestrial and space-based applications. Earlier theoretical calculation have indicated that InGaN-based solar cells can be designed to exhibit a theoretical conversion efficiency of greater than 50% when the In content of the InGaN alloys is about 40%.[6] However, there are several challenges to take full advantage of the potential of InGaN material. Growing InGaN films with both high indium content and enough thickness has proven to be difficult, because the lattice mismatch between GaN and InGaN will induce a high dislocation density,[7−9] leading to an inferior power conversion efficiency.[10,11] For example, Mukhtarova *et al.* investigated that an increase in the number of wells from 5 to 40 improves the overall conversion efficiency from 0.09% to 0.85%; however, further increasing the number of wells to 100 leads to a conversion efficiency increase difficulty or even decreases it to 0.78%.[12] Researchers also reported that the conversion efficiency in $In_{0.28}Ga_{0.72}N$ MQW solar cells (1.02%) is slightly less than that in $In_{0.2}Ga_{0.8}N$ MQW solar cells (1.06%).[13] Therefore, it is necessary to develop strategies to increase the efficiency of solar cells.

The piezo-phototronic effect is a three-way coupling among piezoelectricity, photonic excitation, and semiconductor transport in materials with noncentral symmetric crystal structures, which is due to the presence of piezoelectric charges at two materials' interface.[14−17] Using the inner crystal piezopotential as a "gate" voltage to control electron−hole pair generation, transport, separation, and/or recombination, the electro-optical processes of optoelectronic devices can be effectively

Received: July 13, 2017
Accepted: September 5, 2017
Published: September 5, 2017

DOI: 10.1021/acsnano.7b04935
ACS Nano XXXX, XXX, XXX−XXX

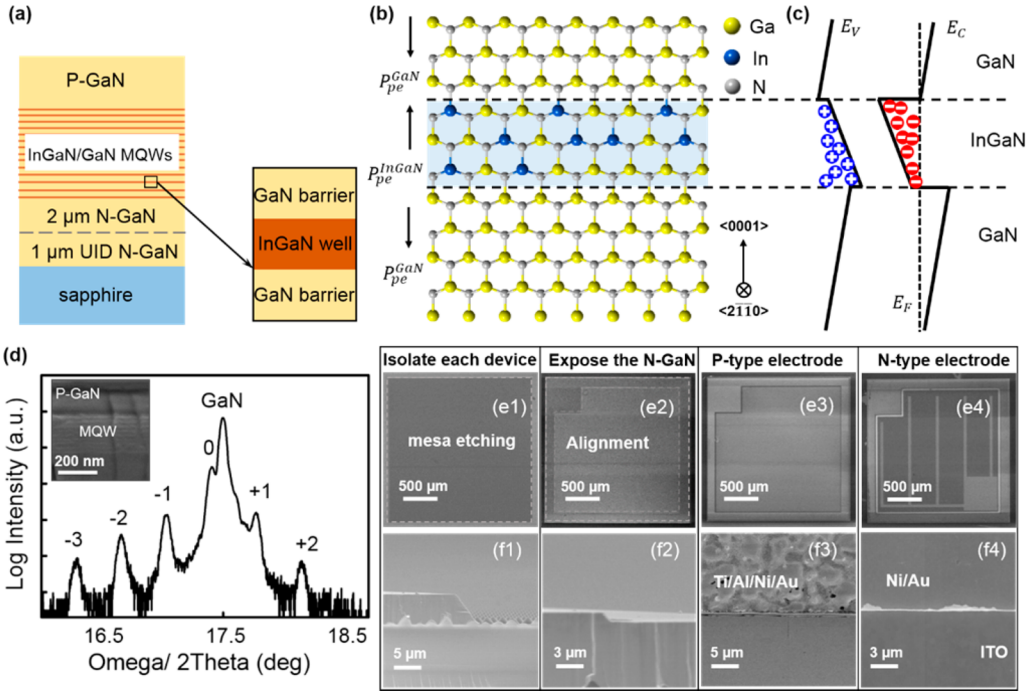

Figure 1. Structural characterization of an InGaN/GaN MQW solar cell. (a) Cross-sectional schematic of the InGaN/GaN MQW solar cell and magnified cross-sectional view of a highlighted GaN/InGaN/GaN heterostructure. Corresponding atomic structure model (b) and energy band diagram (c). (d) High-resolution omega/2theta scans of MQW structures, showing a high crystal quality. The inset is the SEM images of an InGaN/GaN multiple quantum well structure. (e1−e4) SEM images illustrating the fabrication process of the solar cell with a 2 × 2 mm^2 mesa size. (f1, f2) Cross-sectional view of the actual device etched by ICP. The vertical depth is 5 and 1 μm, respectively. (f3, f4) Partial top views of the electrodes.

modulated. This effect has been applied to enhance the sensitivity of bio/chemical sensors,[18−22] the performance of photovoltaic devices,[23,24] and the light-emission efficiency of light-emitting diodes (LEDs).[25−27] These devices can be effectively modulated by applying an external mechanical stress/strain, which leads to a series of optoelectronic phenomena and scientific applications. Most piezo-phototronic devices take a metal−semiconductor (MS) or heterojunction structure, such as ZnO micro/nanowire devices with electric transport characteristics improvement[28] and n-ZnO/p-SnS photocells with a conversion efficiency enhancement.[23] With the development of nanotechnology, the coupling between the piezotronic/piezo-phototronic effect and the quantum confinement gradually becomes possible. The PL intensity modulation of InGaN/GaN MQWs by the piezo-phototronic effect has been presented theoretically and experimentally.[21,29]

In this work, we present the enhancing of InGaN/GaN MQWs' solar cell efficiency by the piezo-phototronic effect. Under external stress, the short-circuit current is increased from 1.05 mA/cm^2 to 1.17 mA/cm^2 and the maximum conversion efficiency of the solar cell is increased from 1.12% to 1.24%, relatively enhanced by 11%. Furthermore, a self-consistent numerical model was established to illustrate the piezo-phototronic effect in an InGaN/GaN multiple quantum well solar cell and offered many important clarifications, including the energy band structure and the optical transition rate. In a word, this study shows that the piezo-phototronic effect offers a feasible way to increase the optical absorption of InGaN/GaN MQW solar cells. Our piezo-phototronic effect modulation is a very simple, recoverable, high-efficient technology to improve the conversion efficiency, which has great potential in the design of nitride solar cells.

RESULTS AND DISCUSSION

The InGaN/GaN MQWs were grown by metal−organic chemical vapor deposition (MOCVD) on (0001)-plane sapphire substrates, and the In content of the InGaN alloys is 25%. The cross-sectional schematic of the MQWs is shown in Figure 1a. The corresponding atomic structure model and energy band bending of the GaN/InGaN/GaN quantum well are shown in Figure 1b and c, respectively. Due to its noncentral symmetric crystal structure, the lattice mismatch induces piezoelectric polarization charges at the InGaN/GaN interfaces. These polarization charges lead to the formation of a triangle-shaped potential well in the InGaN layer and then reduce the absorption coefficient. Figure 1d shows high-resolution omega/2theta scans of MQW structures and SEM images of the InGaN/GaN multiple quantum well structure. The sharp peak is (002) from the substrate (taking the thick GaN layer as the substrate), and the broader peak is (002) from the InGaN/GaN MQWs at a lower angle. The distinct, periodic satellite peak (from −3 to +2) occurring on either side of the InGaN zero-order peak reflects the good crystalline quality. The SEM images illustrate the fabrication process of the InGaN/GaN MQW solar cell, as shown in Figure 1e1−e4. Detailed synthesizing processes of the solar cells are found in the Methods section. First, several 2 × 2 mm^2 patterns were etched from top to bottom through photolithography followed by inductively coupled plasma (ICP, BCl_3/Cl_2 chemistry). These patterns were fabricated for device isolation, and the etched depth was about 5 μm (as shown in Figure 1f1), so that the leakage current of the solar cell can be reduced to around 2 × 10^{-5} A. After that, a "back"-shaped area was etched down about 1 μm to expose the n-GaN for ohmic contact formation and define the active mesa. Circular ohmic contacts were made

DOI: 10.1021/acsnano.7b04935
ACS Nano XXXX, XXX, XXX−XXX

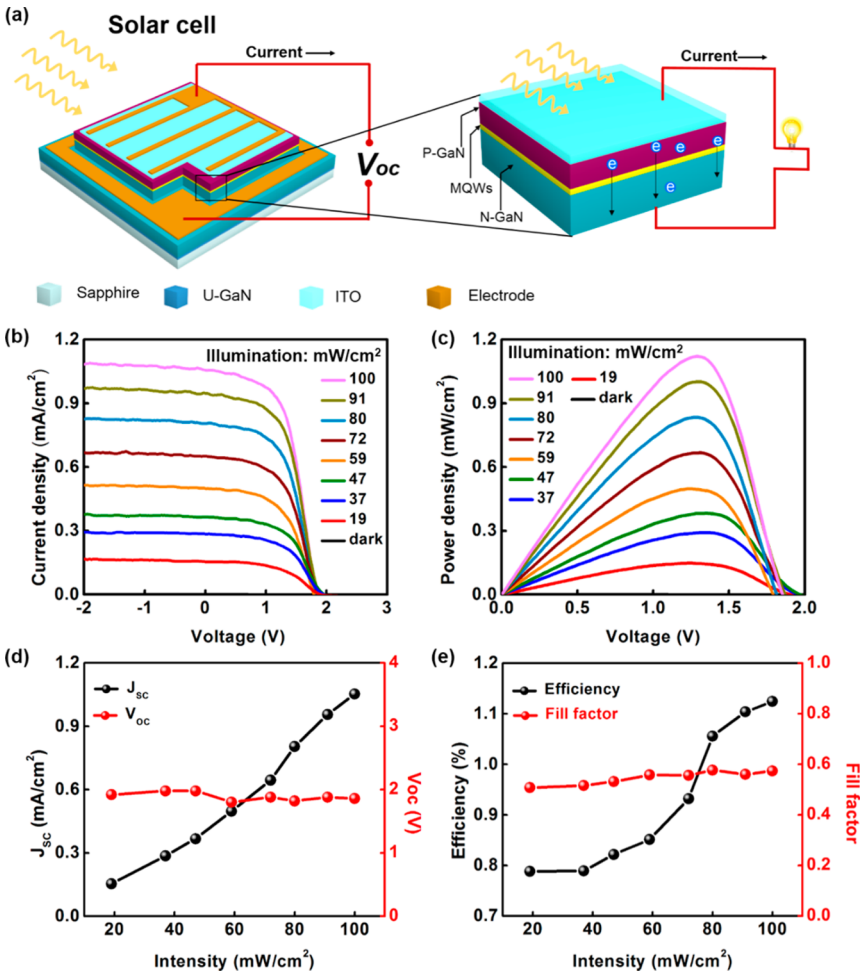

Figure 2. Performances of the InGaN/GaN MQW solar cell under different illumination intensities. (a) Schematic diagram demonstrating the operating principle of the InGaN/GaN MQW solar cell. (b) Room-temperature *J*–*V* characteristics of the InGaN/GaN MQW solar cell under different illumination intensities. (c) *P*–*V* characteristics of the solar cell under different illumination intensities. (d) Short-circuit current density (J_{SC}) and open-circuit voltage (V_{OC}) of the devices as a function of illumination intensities. (e) Solar energy conversion efficiency (η) and fill factor (FF) of the devices as a function of illumination intensities.

by depositing Ti/Al/Ni/Au with an e-beam and annealing at 850 °C for 30 s in a N_2 atmosphere, which is shown in Figure 1f3.[30] Conductive indium tin oxide (ITO) was sputtered at the surface of p-GaN as the current spreading layer, due to its high transparency in the visible spectral region.[31] Finger electrodes (Ni/Au 230 nm) were deposited on the ITO, as shown in Figure 1f4. These designs could effectively decrease contact resistance or parasitic resistance of the structure, which leads to the enhancement of carrier collection and the high fill factor (FF).

The basic operating principle of the InGaN/GaN MQW photovoltaic cell is shown in Figure 2a. In the structure, the electrons flow from p-GaN through the MQW area toward n-GaN with the sunlight incident on the device, are collected by the contacts, and then drive an external circuit. The output voltage of the MQW solar cell is determined by the barrier material, which has a wider band gap, and its short-circuit current is dominated by the width and the number of quantum wells.[32] In Figure 2b,c, the *J*–*V* characteristics and the *P*–*V* characteristics of the InGaN/GaN MQW solar cell were measured under different illumination intensities at room temperature, respectively. As the intensity ranged from 0 to 100 mW/cm^{-2}, the current density increased approximate linearly, and the power density increased. Under air mass 1.5 (1.5 AM) irradiation (100 mW/cm^2), the efficiency of the devices was found to be 1.12% with a short-circuit current density J_{SC} = 1.05 mA/cm^2, open-circuit voltage V_{OC} = 1.9 V, and fill factor FF = 0.57. The fundamental performance characteristics of the solar cell are plotted as functions of the illumination intensity, as shown in Figure 2d and e. The short-circuit current (J_{SC}), the conversion efficiency (η), and the fill factor (FF) exhibit a near-linear dependency on the illumination intensity, while the open-circuit voltage (V_{OC}) is essentially stable with the increase of intensity. This is because the band gap of the InGaN material and the quality of the electrodes determine the V_{OC} of the device, and the photocurrent in this regime depends on the photon flux, the carriers' lifetime, and the carriers' generation rate. The FF approaches 0.52 at 19 mW/cm^2 and increases slightly with illumination intensity, exceeding 0.57 at 100 mW/cm^2. The power conversion efficiency of the solar cell can be expressed as $\eta = V_{OC} \times J_{SC} \times FF/P_{inc}$, where P_{inc} is the incident irradiance per area unit. As is shown in Figure 2e, η slightly increases with an increase in the illumination intensity from 0.8% to 1.12%, which indicates that the more optical-generated carriers are generated under high illumination intensity.[4,23]

DOI: 10.1021/acsnano.7b04935
ACS Nano XXXX, XXX, XXX–XXX

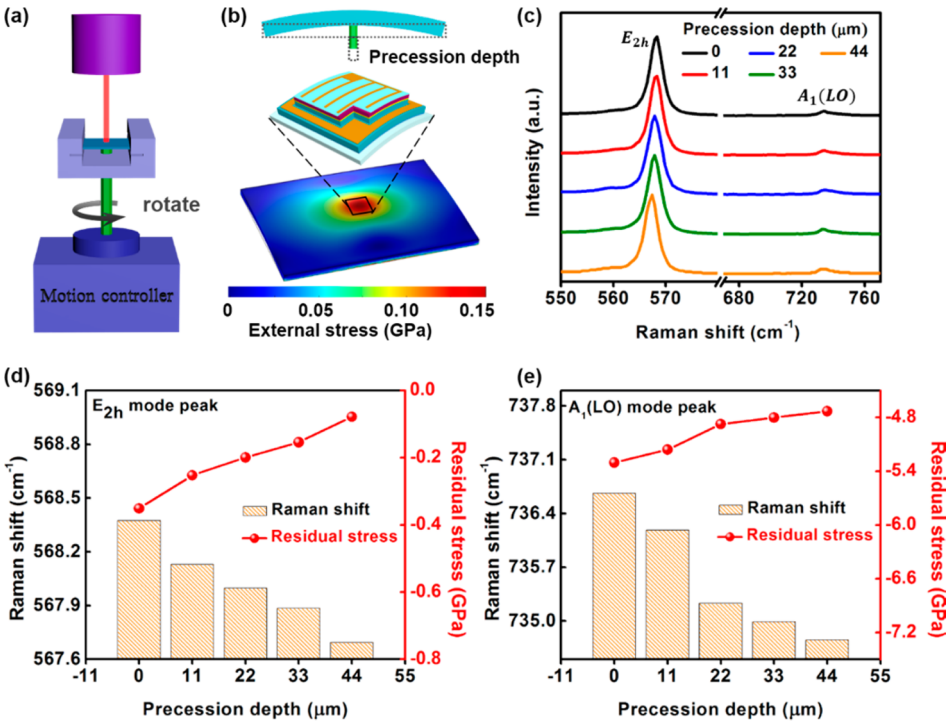

Figure 3. Raman spectra of InGaN/GaN MQWs with various external stress. (a) Schematic diagram of the Raman spectroscopy setup. A metal holder with a jackscrew pinning in the back fixed the sample, and external stress is applied at the sample though the rotation of a motion controller. (b) Stress distribution of the sample induced by the applied stress calculated by COMSOL. The magnitude of the external force is expressed in terms of the precession depth. (c) Dependence of the Raman shift on external stress. The relative Raman shift E_{2h} phonon mode (d) and A_1 (LO) phonon mode (e) of the residual stress in the InGaN/GaN MQWs under different precession depth.

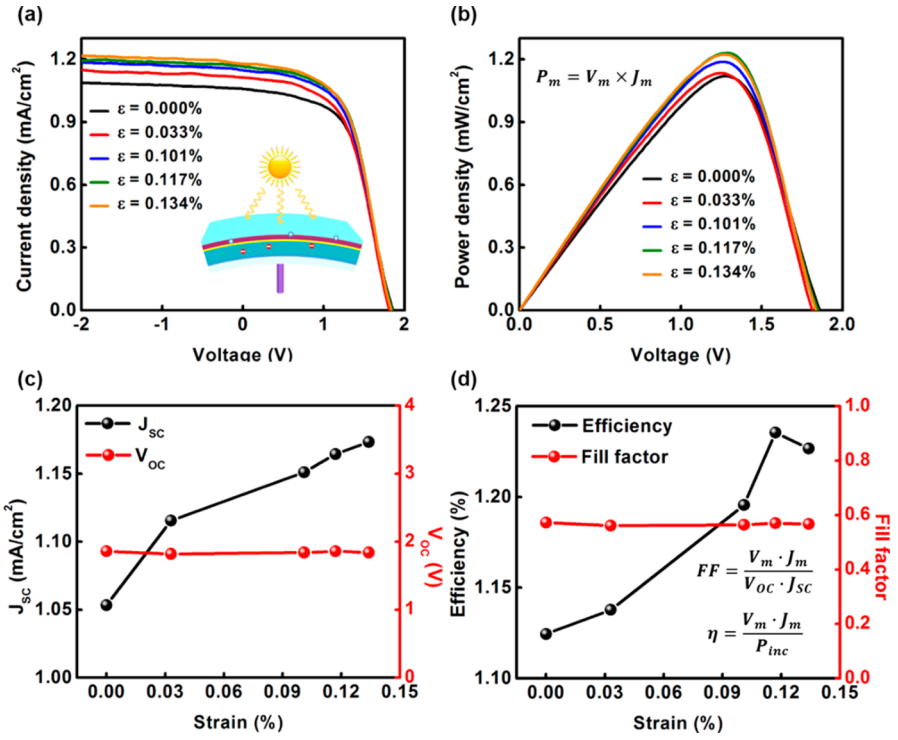

Figure 4. Performances of the solar cell with various external applied strains. (a) $J-V$ characteristics of an InGaN/GaN MQW solar cell under AM 1.5G illumination at different external applied strains. (b) $P-V$ characteristics of the solar cell at different external applied strains. (c) External strain dependence of the short-circuit current density (J_{SC}) and the open-circuit voltage (V_{OC}). (d) External strain dependence of the solar energy conversion efficiency (η) and the fill factor (FF).

Due to the dependency of the phonon frequencies on strain, Raman spectroscopy is a standard technique to investigate the strain in III−V alloy systems.[33] The experimental setup presented in Figure 3a is carried out to investigate the

DOI: 10.1021/acsnano.7b04935
ACS Nano XXXX, XXX, XXX−XXX

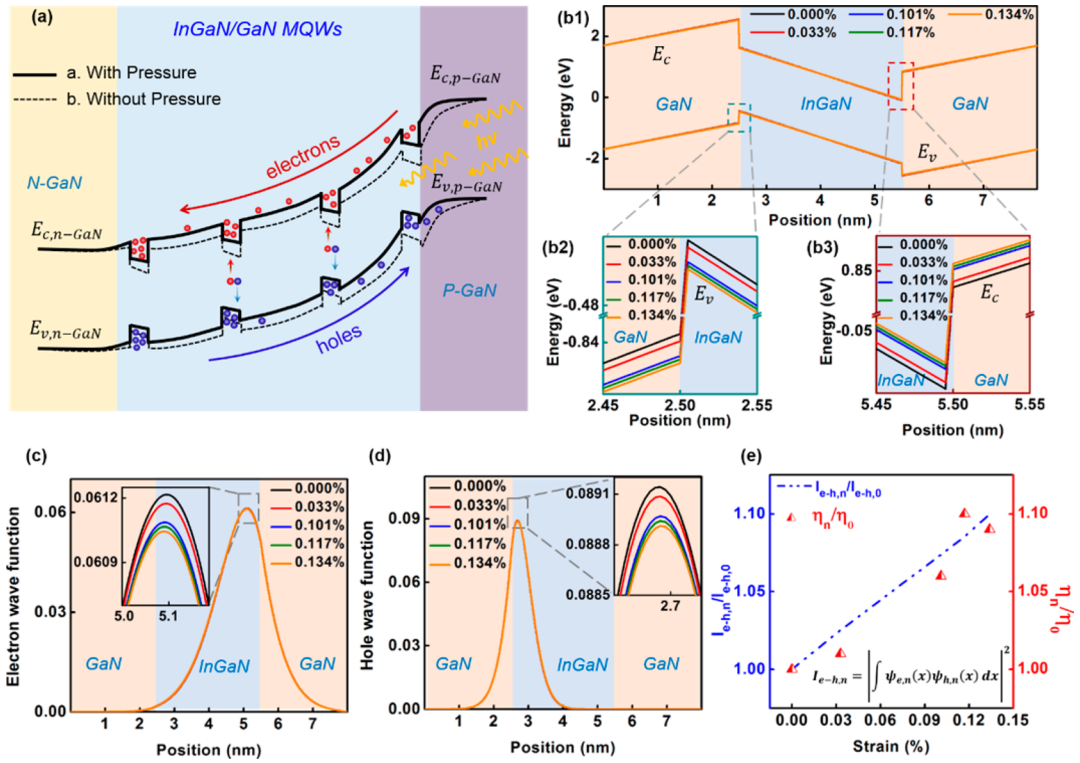

Figure 5. (a) Mechanism of the InGaN/GaN MQW solar cell modulated by the piezo-phototronic effect. The dashed line and solid line indicate the schematic band diagram of the InGaN/GaN MQW structure with and without strain/pressure, respectively. (b1) Calculated energy band profiles of the GaN/InGaN/GaN heterostructure from top to bottom under strain-free and various straining conditions. (b2) Enlarged E_v at the GaN/InGaN heterojunction interface as labeled in (b1) with a green rectangle. (b3) Enlarged E_c at the InGaN/GaN heterojunction interface as labeled in (b1) with a red rectangle. (c) Electron wave function distribution with and without strain (dark line). The inset shows the shifting peak position. (d) Hole wave function distribution with and without strain (dark line). The inset shows the shifting peak position. (e) Normalized square of the spatial overlap of the electron−hole wave functions and the normalized experimental conversion efficiency of the solar cell under strain-free and various straining conditions.

Raman shift of the sample under different external stress. The sample is fixed on a plate by a jig, with a jackscrew pinning locked at the back. The external stress is applied on the device along the *c*-axis direction through a mechanical rotation instrument. The precession depth of the jackscrew reflects the magnitude of the external stress. The stress distribution of the sample induced by the applied stress was calculated by COMSOL 4.3a, as shown in Figure 3b, and the stress was symmetrically distributed in the photovoltaic device with a maximum value of 0.15 GPa at the center of the device. Figure 3c shows the Raman spectra of the sample with and without strain obtained at room temperature. As the precession depth increased, both the E_{2h} mode of GaN and $A_1(LO)$ mode of InGaN shift toward the short wavenumber. The residual compressive stress in wz-GaN was obtained by the relative shift of the E_{2h} phonon mode typically,[34−36] and the relation between the biaxial stress and these relative Raman active phonon modes was described as $\Delta\omega = \omega - \omega_0 = K_{Ph}^{biax}\,\sigma_{xx}$, where ω is the measured peak position, ω_0 is 567.5 cm^{-1} as the standard value for bulk GaN,[37] K_{Ph}^{biax} denotes the stress coefficient assuming biaxial stress in the *c* plane, and σ_{xx} is the residual stress expressed in GPa. In Figure 3d, the Raman shift of the E_{2h} mode of GaN on sapphire and the residual stress in GaN are calculated and plotted as a function of the applied stress (precession depth), and it is noticed that the E_{2h} mode shifts from 568.4 cm^{-1} to 567.7 cm^{-1}, which corresponds to the compressive residual stress from 0.35 GPa to 0.07 GPa. Figure 3e shows the dependence of the $A_1(LO)$ mode of InGaN and the residual stress in InGaN quantum wells on the precession depth. The compressive residual stress of InGaN decreases from 5.30 GPa to 4.73 GPa as the precession depth increases from 0 μm to 44 μm. This reveals that the external stress partly compensates the internal stress induced by lattice mismatch in the InGaN epilayer,[38] and the external applied strain in InGaN increases to 0.134% based on the linear elasticity theory.[29,36]

Figure 4 shows the performance of the InGaN/GaN MQW solar cell modulated by the piezo-phototronic effect. The *J*−*V* characteristics of the solar cell are measured by a solar simulator under AM 1.5 G illumination conditions, as shown in Figure 4a. As the external applied strains increased, the current density of the solar cell was enhanced. The *P*−*V* curves for the device under different strains are shown in Figure 4b, the voltage relative to the maximum power point is essentially constant, while the power increases with an increase in the external strain from 0.000% to 0.134%. To investigate the J_{SC} modulated by the piezo-phototronic effect more clearly, we extracted and plotted the J_{SC} and the V_{OC} under external strains through varying the precession depth as shown in Figure 4c. The open-circuit voltage (V_{OC}) of the solar cell is nearly identical under different external strains, which is because piezoelectric charges were confined at the interfaces and thus did not change the quasi-Fermi level splitting through the solar cell. But the short-circuit current density (J_{SC}) was enhanced significantly from 1.05 mA/cm^2 to 1.17 mA/cm^2, which is related to the enhanced optical absorption. Increasing the optical absorption is the most important issue for the InGaN/GaN solar cell.

DOI: 10.1021/acsnano.7b04935
ACS Nano XXXX, XXX, XXX−XXX

People have taken great efforts to optimize the MOCVD epitaxy technology to grow high-quality InGaN/GaN MQWs with a higher In content and more quantum wells. However, when the number of quantum wells is larger than 40, the conversion efficiency increases with difficulty or even decreases to 0.78%;[12] moreover, the high In-content ($In_{0.28}Ga_{0.72}N$) MQW solar cells exhibit lower conversion efficiency than that in $In_{0.2}Ga_{0.8}N$ MQW solar cells.[13] In our sample, the maximum conversion efficiency of the InGaN/GaN MQW solar cell increases from 1.12% to 1.24%, enhanced by 11% under a 0.134% external strain. As shown in Figure 4d, the FF decreases a bit from 57.3% to 56.7%. When the external strain exceeds 0.117%, the efficiency starts to decrease slightly, which is probably due to more significant lattice scattering. The performances of the solar cell before and after applying the strain are shown in Figure S1 (Supporting Information). It indicates that our piezo-phototronic effect modulation is a very simple and highly efficient technology to improve the performance of the InGaN/GaN MQW solar cell, which has great potential in nitride solar cells.

The piezo-phototronic effect provides a solution to improve the conversion efficiency of the InGaN/GaN MQW solar cells, and the mechanism is discussed below. When an external stress is applied on the InGaN/GaN multiple quantum wells, as shown in Figure 5a, the external-stress-induced piezoelectric charges will be generated at the interfaces of the barrier and well. These charges partly compensate the charges induced by the internal stress in the InGaN wells.[29,39] Therefore, the optical transition is modified by the external stress. To quantitively evaluate the piezo-phototronic effect in the InGaN/GaN MQW solar cell, a self-consistent numerical model was established to calculate the energy band structure and the transition rate in an InGaN/GaN multiple quantum well solar cell. The calculated energy band profiles of the GaN/InGaN/GaN heterostructure under strain-free and straining conditions are shown in Figure 5b1, and the detailed band diagrams at each interface are shown in Figure 5b2 and b3. It becomes obvious that, as the external strain increases, E_v of the GaN/InGaN heterojunction interface decreases while E_c of the InGaN/GaN heterojunction interface trends upward. For the quantum well structure, the lattice-mismatch-induced stress between the quantum barrier and the well is partly compensated by the external stress. Moreover, the electron and hole wave function distributions of the structure with and without strain (dark line) are plotted in Figure 5c and d, and the insets show the shifted peak position, which clearly shows that both the electron and the hole wave function move toward the well. Therefore, the optical absorption in the quantum well is enhanced, resulting in more optical-generated carriers. The optical absorption coefficient is proportional to the square of the spatial overlap of electron−hole wave functions, $I_{e-h,n}$ (n = 0, 1, 2, 3, 4, 0 corresponds to the device under no strain and 1−4 correspond to the device under different external strains).[40] The square of the overlap under different strains relative to $I_{e-h,0}$ is extracted and plotted in Figure 5e, showing that the spatial overlap increases with the increase of the strains. The variation of the $I_{e-h,n}/I_{e-h,0}$ under higher strain is also calculated, which is shown in Figure S2 (Supporting Information). Meanwhile, the relative changes of experimental conversion efficiency for the MQW solar cell η_n/η_0 (n = 0, 1, 2, 3, 4) are displayed, which agree with the calculated results of the spatial overlap of electron−hole wave functions. This suggests that the conversion efficiency of the InGaN/GaN MQW solar cell can be enhanced by the piezo-phototronic effect.

CONCLUSIONS

In summary, the piezo-phototronic effect enhancement of the conversion efficiency of an InGaN/GaN multiple quantum well solar cell was observed. Under 0.134% applied strain, the maximum conversion efficiency of the solar cell is increased by 11%, and the short-circuit current is increased from 1.05 mA/cm^2 to 1.17 mA/cm^2. The physical mechanism was proposed and confirmed *via* a self-consistent numerical model, and the theoretical simulation agreed very well with the experimental measurement. The external stress partly compensates the internal stress induced by the lattice mismatch, which flattens the energy band diagram to increase the spatial overlap of electron−hole wave functions and finally increases the optical absorption. This study provides a scientific and convenient scheme for improving the performance of InGaN/GaN MQW solar cells and holds great promise to maximize the use of solar energy.

METHODS

Fabrication Processes of the Solar Cells. The InGaN/GaN MQW heterostructure, as shown schematically, was grown on a (0001)-patterned sapphire substrate by a MOCVD system. The layer structures consist of 2 μm thick n-type GaN, a nine-period InGaN/GaN (3/13 nm) MQW absorption layer, and a 0.2 μm p-type GaN layer. The predominant electroluminescence emission peak was estimated to occur around 450 nm, corresponding to the $In_{0.25}Ga_{0.75}N$/GaN MQWs (E_g ~2.75 eV). The influence of the MQW structures on the performance of the piezo-phototronic-modulated InGaN solar cells has been investigated by a self-consistent numerical model, as is shown in Figure S3 (Supporting Information). In the device fabrication, a 1.5 μm thick SiO_2 layer was deposited by plasma-enhanced chemical vapor deposition (PECVD) as an etching mask, and a 2 × 2 mm^2 mesa etch was done with an inductively coupled plasma reactive ion etching (ICP-RIE) system until n-GaN was exposed. The remaining SiO_2 sacrificial layer was removed from the p-GaN by immersing them in a hydrogen fluoride (HF) solution and then treated under a power of 300 W O_2 plasma in a reactive ion etching to form an immaculate surface, which facilitates achieving an excellent uniformity for the photoresist spin-coating on the plate. In the coating process, the AZ4620 photoresist was first applied to the device surface by dropper and then high-speed rotated with a speed of 2500 r/min. The thickness of the photoresist was about 3 μm. A mesa region was etched down to n-type GaN about 1 μm deep, so that a Ti/Al/Ni/Au (20/120/45/55 nm) n-contact could be deposited by e-beam evaporation using optical lithography and a lift-off technique. In order to form an ohmic contact, the samples were annealed at 850 °C for 30 s in a rapid thermal annealing machine under a nitrogen (N_2) atmosphere. A 200 nm thick ITO layer was deposited by RF magnetron sputtering on p-GaN as a current spreading layer, followed by annealing in air at 550 °C for 10 min. Finally, Ni/Au (30 nm/200 nm) metal grids were deposited for p-type contacts using dc magnetron sputtering at room temperature.

Optical and Electrical Characterization. The XRD measurement was performed using the Bede D1 system. The microscopic structure was characterized with a Hitachi SU8020 field-emission scanning electron microscope. The Raman measurements were carried out with a micro-Raman spectrometer (LabRam HR Evolution) at room temperature, and the emission wavelength of the laser was 532 nm, with a beam spot size of 1 μm. The solar cells were irradiated using a microprobe station, a solar simulator (model PT-SUN2S, Pharos Technology) with a spectrum distribution of AM 1.5 G, and a Keithley 2450 source meter. The system was calibrated against a standard silicon solar cell to accurately simulate 1 sun intensity (100

DOI: 10.1021/acsnano.7b04935
ACS Nano XXXX, XXX, XXX−XXX

mW/cm^2). The current−voltage characteristics were measured with the Keithley 2450 source meter.

ASSOCIATED CONTENT

Supporting Information

The Supporting Information is available free of charge on the ACS Publications website at DOI: 10.1021/acsnano.7b04935.

Measured $I-V$ curves before and after applying the strain, calculated $I_{e-h,n}/I_{e-h,0}$ under higher strain, and the influence of the MQW structures on the performance of the piezo-phototronic-modulated InGaN solar cells with a self-consistent numerical model (PDF)

AUTHOR INFORMATION

Corresponding Authors

*E-mail: huweiguo@binn.cas.cn.
*E-mail: zlwang@gatech.edu.

ORCID

Weiguo Hu: 0000-0002-8614-0359

Author Contributions

⊥C. Jiang and L. Jing contributed equally to this work.

Notes

The authors declare no competing financial interest.

ACKNOWLEDGMENTS

The authors thank the support from the "Thousands Talents" Program for Pioneer Researcher and His Innovation Team, China, National Natural Science Foundation of China (Grant Nos. 51432005, 61574018, and 51603013), "Hundred Talents Program" of the Chinese Academy of Science, and National Key Research and Development Program of China (2016YFA0202703).

REFERENCES

(1) Li, D.; Sun, X.; Song, H.; Li, Z.; Chen, Y.; Jiang, H.; Miao, G. Realization of a High-Performance GaN UV Detector by Nanoplasmonic Enhancement. *Adv. Mater.* **2012**, *24*, 845−849.

(2) Kurtz, S. R.; Allerman, A. A.; Jones, E. D.; Gee, J. M.; Banas, J. J.; Hammons, B. E. InGaAsN Solar Cells with 1.0 eV Band Gap, Lattice Matched to GaAs. *Appl. Phys. Lett.* **1999**, *74*, 729.

(3) Jani, O.; Honsberg, C.; Huang, Y.; Song, J. o.; Ferguson, I.; Namkoong, G.; Trybus, E.; Doolittle, A.; Kurtz, S. *Design, Growth, Fabrication and Characterization of High-Band Gap InGaN/GaN Solar Cells*; 2006 IEEE 4th World Conference on Photovoltaic Energy Conference, May 2006; pp 20−25.

(4) Dahal, R.; Li, J.; Aryal, K.; Lin, J. Y.; Jiang, H. X. InGaN/GaN Multiple Quantum Well Concentrator Solar Cells. *Appl. Phys. Lett.* **2010**, *97*, 073115.

(5) Lee, S.; Honda, Y.; Amano, H. Effect of Piezoelectric Field on Carrier Dynamics in InGaN-Based Solar Cells. *J. Phys. D: Appl. Phys.* **2016**, *49*, 025103.

(6) Dahal, R.; Pantha, B.; Li, J.; Lin, J. Y.; Jiang, H. X. InGaN/GaN Multiple Quantum Well Solar Cells with Long Operating Wavelengths. *Appl. Phys. Lett.* **2009**, *94*, 063505.

(7) Bi, Z.; Zhang, J.; Hao, Y. *GaN Multiple Quantum Well Solar Cells on a Patterned Sapphire Substrate*; AASRI International Conference on Industrial Electronics and Applications (IEA 2015); Atlantis Press, 2015.

(8) Haghkish, S.; Asgari, A. *The Effects of Cap Layer Thickness on the Performance of InGaN/GaN MQW Solar Cell*. arXiv preprint arXiv:1605.06816, 2016.

(9) Bae, S.-Y.; Jung, B. O.; Lekhal, K.; Lee, D.-S.; Deki, M.; Honda, Y.; Amano, H. Structural and Optical Study of Core-Shell InGaN Layers of Nanorod Arrays with Multiple Stacks of InGaN/GaN Superlattices for Absorption of Longer Solar Spectrum. *Jpn. J. Appl. Phys.* **2016**, *55*, 05FG03.

(10) Horng, R.-H.; Lin, S.-T.; Tsai, Y.-L.; Chu, M.-T.; Liao, W.-Y.; Wu, M.-H.; Lin, R.-M.; Lu, Y.-C. Improved Conversion Efficiency of GaN/InGaN Thin-Film Solar Cells. *IEEE Electron Device Lett.* **2009**, *30*, 724−726.

(11) Sang, L.; Liao, M.; Liang, Q.; Takeguchi, M.; Dierre, B.; Shen, B.; Sekiguchi, T.; Koide, Y.; Sumiya, M. A Multilevel Intermediate-Band Solar Cell by InGaN/GaN Quantum Dots with a Strain-Modulated Structure. *Adv. Mater.* **2014**, *26*, 1414−1420.

(12) Mukhtarova, A.; Valdueza-Felip, S.; Redaelli, L.; Durand, C.; Bougerol, C.; Monroy, E.; Eymery, J. Dependence of the Photovoltaic Performance of Pseudomorphic InGaN/GaN Multiple-Quantum-Well Solar Cells on the Active Region Thickness. *Appl. Phys. Lett.* **2016**, *108*, 161907.

(13) Jeng, M.-J.; Lee, Y.-L.; Chang, L.-B. Temperature Dependences of $In_xGa_{1-x}N$ Multiple Quantum Well Solar Cells. *J. Phys. D: Appl. Phys.* **2009**, *42*, 105101.

(14) Wang, Z. L. Piezopotential Gated Nanowire Devices: Piezotronics and Piezo-Phototronics. *Nano Today* **2010**, *5*, 540−552.

(15) Liu, Y.; Niu, S.; Yang, Q.; Klein, B. D.; Zhou, Y. S.; Wang, Z. L. Theoretical Study of Piezo-Phototronic Nano-LEDs. *Adv. Mater.* **2014**, *26*, 7209−7216.

(16) Wang, Z. L. Progress in Piezotronics and Piezo-Phototronics. *Adv. Mater.* **2012**, *24*, 4632−4646.

(17) Liu, Y.; Zhang, Y.; Yang, Q.; Niu, S.; Wang, Z. L. Fundamental Theories of Piezotronics and Piezo-Phototronics. *Nano Energy* **2015**, *14*, 257−275.

(18) Niu, S.; Hu, Y.; Wen, X.; Zhou, Y.; Zhang, F.; Lin, L.; Wang, S.; Wang, Z. L. Enhanced Performance of Flexible ZnO Nanowire Based Room-Temperature Oxygen Sensors by Piezotronic Effect. *Adv. Mater.* **2013**, *25*, 3701−3706.

(19) Cui, N.; Wu, W.; Zhao, Y.; Bai, S.; Meng, L.; Qin, Y.; Wang, Z. L. Magnetic Force Driven Nanogenerators as a Noncontact Energy Harvester and Sensor. *Nano Lett.* **2012**, *12*, 3701−3705.

(20) Zhao, Z.; Jiang, C.; Pu, X.; Du, C.; Li, L.; Ma, B.; Hu, W. Robust Pb2+ Sensor Based on Flexible ZnO/ZnS Core-Shell Nanoarrays. *Appl. Phys. Lett.* **2016**, *108*, 153104.

(21) Peng, M.; Li, Z.; Liu, C.; Zheng, Q.; Shi, X.; Song, M.; Zhang, Y.; Du, S.; Zhai, J.; Wang, Z. L. High-Resolution Dynamic Pressure Sensor Array Based on Piezo-Phototronic Effect Tuned Photoluminescence Imaging. *ACS Nano* **2015**, *9*, 3143−3150.

(22) Wu, W.; Wang, Z. L. Piezotronics and Piezo-Phototronics for Adaptive Electronics and Optoelectronics. *Nat. Rev. Mater.* **2016**, *1*, 16031.

(23) Zhu, L.; Wang, L.; Xue, F.; Chen, L.; Fu, J.; Feng, X.; Li, T.; Wang, Z. L. Piezo-Phototronic Effect Enhanced Flexible Solar Cells Based on n-ZnO/p-SnS Core-Shell Nanowire Array. *Adv. Sci.* **2017**, *4*, 1600185.

(24) Zhu, L.; Wang, L.; Pan, C.; Chen, L.; Xue, F.; Chen, B.; Yang, L.; Su, L.; Wang, Z. L. Enhancing the Efficiency of Silicon-Based Solar Cells by the Piezo-Phototronic Effect. *ACS Nano* **2017**, *11*, 1894−1900.

(25) Peng, M.; Zhang, Y.; Liu, Y.; Song, M.; Zhai, J.; Wang, Z. L. Magnetic-Mechanical-Electrical-Optical Coupling Effects in GaN-Based LED/Rare-Earth Terfenol-D Structures. *Adv. Mater.* **2014**, *26*, 6767−6772.

(26) Pan, C.; Dong, L.; Zhu, G.; Niu, S.; Yu, R.; Yang, Q.; Liu, Y.; Wang, Z. L. High-Resolution Electroluminescent Imaging of Pressure Distribution Using a Piezoelectric Nanowire LED Array. *Nat. Photonics* **2013**, *7*, 752−758.

(27) Tsai, S.-C.; Lu, C.-H.; Liu, C.-P. Piezoelectric Effect on Compensation of the Quantum-Confined Stark Effect in InGaN/GaN Multiple Quantum Wells Based Green Light-Emitting Diodes. *Nano Energy* **2016**, *28*, 373−379.

(28) Hu, Y.; Chang, Y.; Fei, P.; Snyder, R. L.; Wang, Z. L. Designing the Electric Transport Characteristics of ZnO Micro/Nanowire Devices by Coupling Piezoelectric and Photoexcitation Effects. *ACS Nano* **2010**, *4*, 1234−1240.

DOI: 10.1021/acsnano.7b04935
ACS Nano XXXX, XXX, XXX−XXX

(29) Huang, X.; Du, C.; Zhou, Y.; Jiang, C.; Pu, X.; Liu, W.; Hu, W.; Chen, H.; Wang, Z. L. Piezo-Phototronic Effect in a Quantum Well Structure. *ACS Nano* **2016**, *10*, 5145−5152.
(30) Chern, K. T.; Allen, N. P.; Ciarkowski, T. A.; Laboutin, O. A.; Welser, R. E.; Guido, L. J. GaInN/GaN Solar Cells Made Without P-Type Material Using Oxidized Ni/Au Schottky Electrodes. *Mater. Sci. Semicond. Process.* **2016**, *55*, 2−6.
(31) Bai, J.; Athanasiou, M.; Wang, T. Effect of an ITO Current Spreading Layer on the Performance of InGaN MQW Solar Cells. *Phys. Status Solidi C* **2016**, *13*, 297−300.
(32) Zhang, X.-B.; Wang, X.-L.; Xiao, H.-L.; Yang, C.-B.; Hou, Q.-F.; Yin, H.-B.; Chen, H.; Wang, Z.-G. InGaN/GaN Multiple Quantum Well Solar Cells with an Enhanced Open-Circuit Voltage. *Chin. Phys. B* **2011**, *20*, 028402.
(33) Hernández, S.; Cuscó, R.; Pastor, D.; Artús, L.; O'Donnell, K. P.; Martin, R. W.; Watson, I. M.; Nanishi, Y.; Calleja, E. Raman-Scattering Study of the InGaN Alloy over the Whole Composition Range. *J. Appl. Phys.* **2005**, *98*, 013511.
(34) Kozawa, T.; Kachi, T.; Kano, H.; Nagase, H.; Koide, N.; Manabe, K. Thermal Stress in GaN Epitaxial Layers Grown on Sapphire Substrates. *J. Appl. Phys.* **1995**, *77*, 4389−4392.
(35) Paskova, T.; Hommel, D.; Paskov, P. P.; Darakchieva, V.; Monemar, B.; Bockowski, M.; Suski, T.; Grzegory, I.; Tuomisto, F.; Saarinen, K.; Ashkenov, N.; Schubert, M. Effect of High-Temperature Annealing on the Residual Strain and Bending of Freestanding GaN Films Grown by Hydride Vapor Phase Epitaxy. *Appl. Phys. Lett.* **2006**, *88*, 141909.
(36) Röder, C. *Strain, Charge Carriers, and Phonon Polaritons in Wurtzite GaN-a Raman Spectroscopical View*. Ph.D. Thesis, Technische Universitat Bergakademie Freiberg, Freiberg, 2014, pp 39−41.
(37) Perlin, P.; Jauberthie-Carillon, C.; Itie, J. P.; San Miguel, A.; Grzegory, I.; Polian, A. Raman Scattering and X-Ray-Absorption Spectroscopy in Gallium Nitride Under High Pressure. *Phys. Rev. B: Condens. Matter Mater. Phys.* **1992**, *45*, 83−89.
(38) Wagner, J.; Ramakrishnan, A.; Obloh, H.; Maier, M. Effect of Strain and Associated Piezoelectric Fields in InGaN/GaN Quantum Wells Probed by Resonant Raman Scattering. *Appl. Phys. Lett.* **1999**, *74*, 3863−3865.
(39) Huang, X.; Jiang, C.; Du, C.; Jing, L.; Liu, M.; Hu, W.; Wang, Z. L. Enhanced Luminescence Performance of Quantum Wells by Coupling Piezo-Phototronic with Plasmonic Effects. *ACS Nano* **2016**, *10*, 11420−11427.
(40) Smith, D. L.; Mailhiot, C. k·p Theory of Semiconductor Superlattice Electronic Structure. I. Formal Results. *Phys. Rev. B: Condens. Matter Mater. Phys.* **1986**, *33*, 8345−8359.

DOI: 10.1021/acsnano.7b04935
ACS Nano XXXX, XXX, XXX−XXX